IEEE Access
Multidisciplinary | Rapid Review | Open Access Journal

Received July 26, 2021, accepted August 7, 2021, date of publication August 9, 2021, date of current version August 25, 2021.

Digital Object Identifier 10.1109/ACCESS.2021.3103883

Clipping Noise Mitigation in Optical OFDM Using Decision-Directed Signal Reconstruction

CUIWEI HE AND YUTO LIM, (Member, IEEE)
School of Information Science, Japan Advanced Institute of Science and Technology, Nomi 923-1211, Japan
Corresponding author: Cuiwei He (cuiweihe@jaist.ac.jp)

ABSTRACT In this paper, the performance of a new decision-directed signal reconstruction (DDSR) algorithm with optimal reconstruction thresholds for use with optical orthogonal frequency division multiplexing (OFDM) modulation is investigated. Clipping noise remains one of the main drawbacks in many practical optical OFDM transmission systems. It has been shown in previous studies that a time-domain based DDSR algorithm can be used to effectively reduce the clipping noise. However, in all existing works studying this DDSR algorithm, the decision threshold used to direct the time-domain signal reconstruction is fixed and equal to the level at which the transmitted signal is clipped. In this paper, it is shown that, due to the influences of the unavoidable noise at the receiver, fixing the DDSR threshold at the clipping level is not an optimal solution and can severely limit the advantages of using this algorithm. A detailed theoretical analysis is performed to investigate the key factors that influence the choices of the optimal DDSR thresholds. The presented simulation results are used to verify the accuracy of the theoretical analysis and also show that the performance of the DDSR algorithm is significantly improved by using the obtained optimal thresholds.

INDEX TERMS Optical wireless communication, optical OFDM, clipping noise, DDSR.

I. INTRODUCTION

Orthogonal frequency division multiplexing (OFDM) is increasingly being used as the modulation method for the next generation intensity modulated/direct detection (IM/DD) based optical wireless communication (OWC) systems [1]–[3]. Because the intensity of light can only be real and positive, a number of unipolar forms of optical OFDM have been developed [4]–[15]. The best known of these are asymmetrically clipped optical OFDM (ACO-OFDM) [4] and DC-biased OFDM (DCO-OFDM) [5]. In ACO-OFDM, only odd subcarriers are loaded with data and therefore the time-domain signal is antisymmetric. When the transmitted signal is clipped at a zero level, the clipping noise only presents on even subcarriers and consequently does not cause signal distortion. However, as only the odd subcarriers are used for data carrying, ACO-OFDM is very inefficient in terms of bandwidth [12]–[16]. In DCO-OFDM, a bipolar OFDM signal is first generated and then a DC bias is added. Next, any remaining negative peaks are clipped to generate a non-negative signal. Because the added DC bias does not carry data, adding a high DC bias is very power inefficient [5]. However, when the added DC bias level is too low, the non-linear clipping operation introduces significant signal distortion which results in data detection errors [5], [17], [18].

One approach to improve the performance of optical OFDM is to design spectral efficient ACO-OFDM where the even subcarriers are used to carry additional data. In [5], a modulation technique named asymmetrically clipped DC-biased optical OFDM (ADO-OFDM) is presented in which the odd subcarriers are used to transmit an ACO-OFDM signal and the even subcarriers are modulated with a DCO-OFDM signal. A similar method has been studied in [6] where the even subcarriers are used to transmit pulse-amplitude-modulated discrete multitone modulation (PAM-DMT) signals [7]. To further enhance the overall performance, Layered ACO-OFDM (LACO-OFDM) is introduced in [12]–[15]. In LACO-OFDM, multiple 'layers' of ACO-OFDM are configured to exploit the use of the even subcarriers. However, the main drawback of this layered or hybrid modulation approach is that the data decoding procedure is a successive interference cancellation process and the computational complexity increases dramatically when the number of layer increases. Moreover, to prevent error propagation, complex coding or signal processing methods [12], [19], [20] are usually required.

The associate editor coordinating the review of this manuscript and approving it for publication was Mohamed M. A. Moustafa.

Another approach to improve the performance of optical OFDM is to use a decision-directed signal reconstruction (DDSR) algorithm which mitigates the clipping noise. In this algorithm, the receiver makes preliminary decisions about the transmitted data and from these constructive information of the original unclipped signal is extracted and then processed together with the received signal to perform more accurate data detections. This method was originally developed for radio frequency (RF) wireless applications and implemented in both the time domain [21] and the frequency domain [22]. It was later adapted for applications to optical OFDM in [23] and [24]. Both the time-domain and the frequency-domain based DDSR methods can be used as an iterative process to improve the estimation accuracy. In [25], it shows that a single shrinkage correction step can be used in place of the iterative process without any reduction in performance.

Although the time-domain and the frequency-domain based DDSR methods are fundamentally very similar, they process the clipped signal in slightly different ways and thus have different performance which has been studied and compared in [26]. In the frequency-domain based method, a time-domain signal is first regenerated after performing preliminary decisions. This regenerated signal is then clipped at the same level as the transmitted signal to estimate the clipping noise in the frequency domain which is next linearly subtracted from the original received signal before performing the final data detections. The potential drawback of this approach is that all constellations of the estimated clipping noise are subjected to the influences of the errors made in the preliminary decisions. When they are linearly removed from the received signal, all resulting signal constellations are influenced by both the detection errors and the receiver noise. In the time-domain based DDSR method, the signal component removed by the clipping operation is first estimated based on the preliminary decisions about the transmitted data. Then it is combined with the original received signal in the time domain which consequently reduces the influence of the clipping noise. However, unlike the frequency-domain based approach in which the estimated clipping noise is linearly subtracted from the received signal, the time-domain signal reconstruction step is a nonlinear process and based on a DDSR threshold. In this process, the signal samples are scanned one by one and compared to the DDSR threshold to be decided for updating or not. Using this approach, the updated signal samples are only affected by the decision errors and the signal samples which are not updated/replaced are only influenced by the receiver noise. To make the best of this method, all clipped signal samples are required to be updated.

However, in all the existing works studying this DDSR algorithm [21], [23], [25]–[28], particularly the time-domain method, the threshold used to direct/guide the time-domain signal reconstruction is fixed at a level at which the signal was clipped at the transmitter. This is arguably the optimal approach when the clipping distortion is the only impairment. However, due to the unavoidable noise at the receiver, a large number of clipped signal samples are above this signal reconstruction threshold and these signal samples cannot be successfully processed or updated. Consequently, in any practical transmission systems, the approach considered in [21], [23], and [25]–[28] is not an optimal solution and can severely degrade the advantages of using this algorithm for mitigating the clipping distortion.

In this paper, a new approach of using the DDSR algorithm is studied. We first analyze the properties of the DCO-OFDM signal and show how the optical power and the clipping distortion of the transmitted signal depend on the clipping levels. Then, we study the symbol error rate (SER) performance of the conventional DCO-OFDM receiver in which the detected signal is affected by both the clipping operation at the transmitter and the noise generated at the receiver. Furthermore, we show how the decision errors introduced in the frequency domain based on the maximum likelihood (ML) criterion affect the regenerated time-domain signal sequence. The optimal threshold for the DDSR algorithm is then determined by analyzing the theoretical signal-to-noise ratio (SNR) of the reconstructed signal. Moreover, each stage of the theoretical analysis is verified using Monte Carlo simulations. The results show that the SNR of the processed signal significantly depends on the choice of the DDSR threshold. The optimal threshold which maximizes the SNR is shown to be dependent on a range of parameters including the noise power, the constellation size and the clipping level. More importantly, we show that the BERs decrease dramatically by using the obtained optimal threshold.

This paper shows many new viewpoints of using the DDSR algorithm for mitigating the clipping noise in optical OFDM systems. It makes a number of important new contributions which include:

1) A detailed analysis which studies how the clipping distortion and the transmitted optical power are affected by both the top clipping and the bottom clipping. Moreover, by calculating the optical power, it is shown that the top of the signal is usually clipped much less than its bottom.
2) Derivation of the detection error probability when the OFDM signal is affected by both the nonlinear clipping operation and the receiver noise.
3) The study of a new type of time-domain noise which is caused by the detection errors in the frequency-domain using ML decoders.
4) Both theoretical SNR analysis and BER simulation results showing how the overall system performance is related to a range of parameters and what parameters can support the optimal performance.

The rest of the paper is structured as follows. Section-II summarizes DCO-OFDM modulation and also studies the related clipping distortion. Section-III introduces the DDSR algorithm for clipping noise mitigation with a flexible signal reconstruction threshold. The noise in the regenerated time-domain signal sequence is then modelled and analyzed

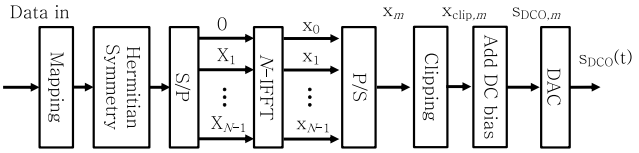

FIGURE 1. The block diagram of the DCO-OFDM transmitter.

in Section-IV. Section-V shows how the theoretical SNR is related to the choice of the signal reconstruction threshold. The simulated BERs in Section-VI are presented to verify the theoretical analysis and show the advantages of using the optimal signal reconstruction threshold. Finally, Section-VII concludes the paper.

II. SYSTEM DESCRIPTION

In this section, we describe the DCO-OFDM transmitter and calculate the expressions for the clipping distortion in the transmitted signal. These analyses include the calculations of the optical power, the shrinkage ratio and the variance of the clipping noise. Fig. 1 shows a typical DCO-OFDM transmitter. The vector, $\mathbf{X} = [X_0, X_1, \ldots, X_{N-1}]$, which is input to the IFFT is a bipolar complex vector representing the QAM modulated data which is to be transmitted, and N is the number of subcarriers. $\mathbf{X}$ is constrained to have Hermitian symmetry, i.e. $X_k = X^*_{N-k}$ for $0 < k < N/2$. The zeroth and Nyquist subcarrier are also set to zero i.e. $X_0 = X_{N/2} = 0$. The output of the IFFT is the real vector, $\mathbf{x} = [x_0, x_1, \ldots, x_{N-1}]$, where

$$x_m = \frac{1}{\sqrt{N}} \sum_{k=0}^{N-1} X_k \exp\left(\frac{j2\pi km}{N}\right), \quad \text{for } 0 \le m \le N-1 \tag{1}$$

In the following, we assume that N is large, so that central limit theorem applies and x_m is approximately Gaussian distributed with zero mean and variance of σ^2. Using the specific form of the IFFT operation shown in (1) which has a coefficient of $1/\sqrt{N}$, the discrete signals at the input and the output of the transform have the same average power [1]. This has many important advantages and also simplifies the analysis of many OFDM functions. In this case,

$$\sigma^2 = E(x_m^2) = E(|X_k|^2) \tag{2}$$

which is also calculated in Appendix-A.

A. CLIPPING OPERATION

In most of the research works [5], [17], [29], [30], the time domain DCO-OFDM signal, x_m, is clipped at its bottom at a level of $-B_{\text{DC}}$ and the clipped signal, $x_{\text{clip},m}$ is given by

$$x_{\text{clip},m} = \begin{cases} -B_{\text{DC}}, & \text{if } x_m \le -B_{\text{DC}} \\ x_m, & \text{if } x_m > -B_{\text{DC}} \end{cases} \tag{3}$$

However, the top of the signal may also be clipped to reduce the dynamic range of the signal in some systems. This may reduce the constraints on the design of the amplifier and/or the resolution of the digital-to-analog convertor (DAC) and/or the linearity of the LED or laser and/or the received signal resolution in photon counting based detection systems [31]–[34]. A more general double-sided clipping operation is given by

$$x_{\text{clip},m} = \begin{cases} -B_{\text{DC}}, & \text{if } x_m < -B_{\text{DC}} \\ x_m, & \text{if } -B_{\text{DC}} \le x_m \le \lambda \\ \lambda, & \text{if } x_m > \lambda \end{cases} \tag{4}$$

where λ is the top level at which the signal is clipped. The PDF of the clipped signal becomes [5]

$$p_{x_{\text{clip}}}(x) = \frac{1}{\sqrt{2\pi}\sigma} \exp\Big(-\frac{x^2}{2\sigma^2}\Big)u(x) + Q\Big(\frac{B_{\text{DC}}}{\sigma}\Big)\delta(x + B_{\text{DC}}) + Q\Big(\frac{\lambda}{\sigma}\Big)\delta(x - \lambda) \tag{5}$$

where

$$u(x) = \begin{cases} 0, & \text{if } x < -B_{\text{DC}} \\ 1, & \text{if } -B_{\text{DC}} \le x \le \lambda \\ 0, & \text{if } x > \lambda \end{cases} \tag{6}$$

$\delta(v)$ is the well-known Dirac delta function and $Q(v) = \frac{1}{\sqrt{2\pi}} \int_v^{+\infty} \exp\left(-\frac{t^2}{2}\right) dt$ is the Q-function. Next, a DC bias, B_{DC}, is added onto $x_{\text{clip},m}$ to generate a positive signal, $s_{\text{DCO},m}$, using

$$s_{\text{DCO},m} = x_{\text{clip},m} + B_{\text{DC}}. \tag{7}$$

Finally, a DAC converts the clipped discrete time domain signal, $s_{\text{DCO},m}$, into an analog signal, $s_{\text{DCO}}(t)$, to drive the transmitter.

B. CLIPPING DISTORTION

In IM/DD based optical transmission systems, the non-linear clipping operation discussed in Section-II-A usually has two functions. First, to generate a unipolar signal, the transmitted signal is typically clipped at its bottom to avoid adding a high DC bias which is very power inefficient. Second, the clipping operation also reduces the peak-to-average power ratio (PAPR) of the transmitted signal which is usually a problem in OFDM. However, at the same time, the nonlinear clipping causes both in-band signal distortion and out-of-band power emission [35]. In RF communications, the spectrum resources are carefully managed and the requirements on the out-of-band emission are usually very strict. However, in optical wireless communication, its spectrum is license free. More importantly, the out-of-band emission is generated in the electrical domain and does not cause interference between optical signals. Consequently, as discussed in [1], the out-of-band power emission is much less of a problem in OWC than in RF communications. In this paper, we also focus on studying methods which can be used to mitigate the in-band signal distortion. To analyze the signal distortion in a more general way, a bottom clipping ratio is set relative to σ by

$$\mu = \frac{B_{\text{DC}}}{\sigma} \tag{8}$$

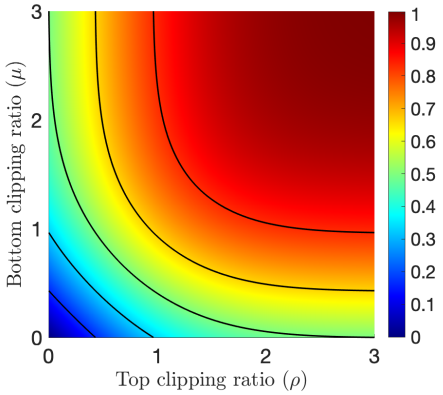

FIGURE 2. The shrinkage factor, α plotted as a function of ρ and μ.

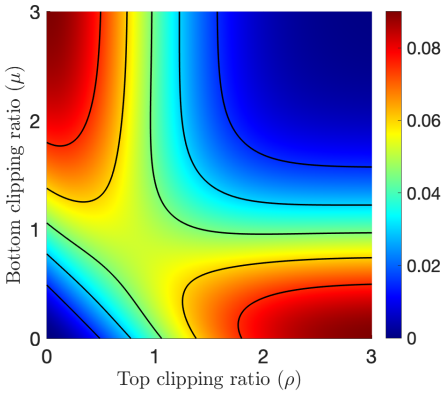

FIGURE 3. The variance of the clipping noise, σ_c^2, plotted as a function of ρ and μ.

and a top clipping ratio is defined as

$$\rho = \frac{\lambda}{\sigma} \tag{9}$$

According to Bussgang' theory [36], the non-linear clipping operation in (4) would both attenuate the signal and cause clipping noise. The clipped signal, $x_{\text{clip},m}$, can be rewritten as

$$x_{\text{clip},m} = \alpha x_m + c_m \tag{10}$$

where α is the shrinkage ratio and c_m is the clipping noise. When the signal is double-sided clipped, based on Bussgang's theory, the shrinkage ratio can be calculated using

$$\begin{aligned}\alpha &= \frac{E(x_{\text{clip},m}x_m)}{E(x_m x_m)} \\ &= \frac{1}{\sigma^2}\int_{-\infty}^{+\infty} x_m x_{\text{clip},m} p_{x_{\text{clip}}}(x)dx \\ &= 1 - Q\left(\frac{B_{DC}}{\sigma}\right) - Q\left(\frac{\lambda}{\sigma}\right) \\ &= 1 - Q(\mu) - Q(\rho)\end{aligned} \tag{11}$$

Using (11), α is plotted as a function of ρ and μ and shown in Fig. 2. We can see that increasing ρ or μ reduces the clipping distortion and thus results in a larger value of α. It also can be noticed that, when both ρ and μ are large (e.g. $\rho = \mu = 3$), α is very close to one because the removed signal due to the clipping operation becomes very limited. When both ρ and μ are zeros, the transmitted signal is completely removed and α is therefore zero. When one side of the transmitted signal is completely clipped and another side is unclipped (e.g. $\rho = 0$ and $\mu = 3$), α is 0.5.

Next, the variance of the double-sided clipping noise, σ_c^2, is studied. σ_c^2 is calculated in Appendix-B and given by (12), as shown at the bottom of the page. It is shown in (12) that σ_c^2 depends on σ^2, ρ and μ. Based on this relationship, σ_c^2 is plotted as a function of ρ and μ with σ^2 fixed at one in Fig. 3. It can be seen that σ_c^2 equals zero when both ρ and μ are zeros or when both ρ and μ are very high (e.g. $\rho = \mu = 3$). This is because when ρ and μ are very high, the removed signal due to clipping is negligible which results in an extremely small value of σ_c^2. When ρ and μ are zeros, the transmitted signal, $x_{\text{clip},m}$, is completely removed. In this case, since α is zero as shown in Fig. 2, the clipping noise part, c_m, does not exist based on (10) and consequently σ_c^2 is zero. It is interesting to notice that, unlike DCO-OFDM with single-sided clipping in which the variance of the clipping noise would become higher when the clipping ratio increases [25], increasing the clipping ratio does not mean σ_c^2 would be increased in a double-sided clipping case.

C. OPTICAL POWER

In IM/DD based OWC systems, the optical power is a very important parameter when the overall performance of the system is investigated. Because intensity modulation is used, the optical power and hence the optical energy per bit depends on the *mean* of the transmitted signal not its *variance*. Based on the statistical properties of the DCO-OFDM signal, the transmitted optical power is calculated in Appendix-B and given by

$$\begin{aligned}P_{\text{opt}} &= \int_{-\infty}^{+\infty} x p_{x_{\text{clip}}}(x)dx + B_{\text{DC}} \\ &= \sigma\left\{\rho Q(\rho) - \mu[Q(\mu) - 1]\right. \\ &\quad \left. - \frac{1}{\sqrt{2\pi}}\left[\exp\left(-\frac{\rho^2}{2}\right) - \exp\left(-\frac{\mu^2}{2}\right)\right]\right\}\end{aligned} \tag{13}$$

$$\begin{aligned}\sigma_c^2 = \sigma^2\Bigg\{&\mu^2 Q(\mu) + \rho^2 Q(\rho) - \frac{1}{\sqrt{2\pi}}\left(\rho\exp\left(-\frac{\rho^2}{2}\right) + \mu\exp\left(-\frac{\mu^2}{2}\right)\right) \\ &- \left[\rho Q(\rho) - \mu Q(\mu) - \frac{1}{\sqrt{2\pi}}\left(\exp\left(-\frac{\rho^2}{2}\right) - \exp\left(-\frac{\mu^2}{2}\right)\right)\right]^2 + \alpha(1-\alpha)\Bigg\}\end{aligned} \tag{12}$$

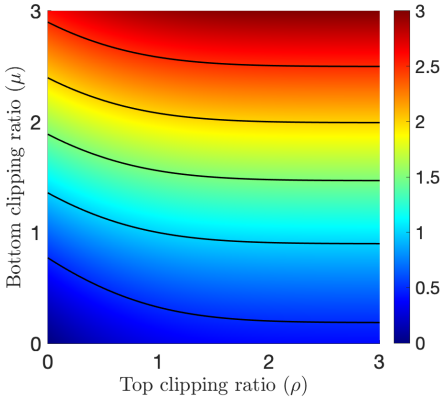

FIGURE 4. The optical power of the transmitted signal plotted as a function of ρ and μ.

In Fig. 4, the optical power of the transmitted signal is plotted as a function of ρ and μ with σ fixed at one. It can seen that the transmitted power is directly related to the amount of clipping at the bottom of the signal. This is because increasing μ means that a large DC bias is required to make the transmitted signal unipolar. By contrast, clipping at the top of the signal does not affect the bias and therefore the average optical power very much. So, to design a more power efficient transmission system without introducing much signal distortion, there is usually an imbalance between the top clipping and the bottom clipping. Typically, clipping at the top of the signal is much less than clipping at the bottom and so has little effect on performance [25]. Consequently, without loss of generality, the cases with single-sided bottom clipping are considered in the following parts of this paper.

In the following analysis, when the single-sided clipping shown in (3) is considered, the PDF of $x_{\text{clip},m}$ becomes

$$p_{x_{\text{clip}}}(x)=\frac{1}{\sqrt{2\pi}\sigma}\exp\Big(-\frac{x^2}{2\sigma^2}\Big)h(x)+Q\Big(\frac{B_{\text{DC}}}{\sigma}\Big)\delta(x+B_{\text{DC}}) \tag{14}$$

where

$$h(x)=\begin{cases}0, & \text{if } x\le -B_{\text{DC}}\\ 1, & \text{if } x> -B_{\text{DC}}\end{cases} \tag{15}$$

The shrinkage ratio, α, and the variance of the clipping noise, σ_{c}^2, shown in (11) and (12) can be simplified as (16) and (17), as shown at the bottom of the page, after removing the terms which are associated with ρ [17]. β in (17) is a function of the clipping ratio and used in later calculations.

$$\alpha=1-Q\Big(\frac{B_{\text{DC}}}{\sigma}\Big)=1-Q(\mu) \tag{16}$$

TABLE 1. OFDM parameters considered in the analysis.

Parameter	Value
Subcarrier number, N	64, 128, 256, 512
Constellation size, M	4-QAM, 16-QAM
Clipping ratio, μ	0.5, 1, 2,3
DC bias level (in dB)	1,3,4, 6

III. DCO-OFDM RECEIVER WITH DDSR

In this section, we describe a generalized DDSR algorithm which is used to effectively mitigate the non-linear clipping distortion. In most of the OWC systems, the generated noise at the receiver is mainly the shot noise caused by the ambient light and/or the thermal noise due to the electronics. These two types of noise can be well modelled as additive white Gaussian noise (AWGN)[1] [37], [38]. In this paper, an AWGN channel is also considered. Although this model does not consider fading, frequency selectivity, interference, it is still extremely useful for gaining insight into the underlying behaviour of the overall system. Moreover, many of the conclusions and analyses can be easily adapted to a system when other factors are considered. In the following, the received signal is given by

$$y(t)=s_{\text{DCO}}(t)+n(t) \tag{18}$$

where $n(t)$ is AWGN. The variance of the noise is σ_{n}^2 and its PDF is given by

$$p_{\text{n}}(x)=\frac{1}{\sqrt{2\pi}\sigma_{\text{n}}}\exp\left(-\frac{x^2}{2\sigma_{\text{n}}^2}\right). \tag{19}$$

The related OFDM parameters considered in this paper in the following analysis are summarized in Table 1.

A. CONVENTIONAL DCO-OFDM RECEIVER

The performance of a conventional DCO-OFDM receiver depends on the details of the receiver design and in particular whether the receiver corrects for the signal attenuation due to clipping. In most papers on DCO-OFDM, no compensation is made for the constellation shrinkage that results from this attenuation and the clipping noise is treated as independent additive noise. However, in practice, channel estimation is based on transmitted pilot signals or known preambles. In this

[1]Note that, in photon counting based OWC systems (e.g. when single photon avalanche diodes (SPADs) are used in the detector), the noise due to the ambient light or the signal itself is Poisson rather than Gaussian. However, in this paper, we consider the more commonly used silicon positive-intrinsic-negative (PIN) photodiode and thus the noise is signal-independent and AWGN is a more suitable noise model.

$$\sigma_{\text{c}}^2=\sigma^2\underbrace{\left\{(1+\mu^2)\Big[Q(\mu)-Q^2(\mu)\Big]-\frac{1}{2\pi}\exp(-\mu^2)-\frac{\mu}{\sqrt{2\pi}}[1-2Q(\mu)]\exp\left(-\frac{\mu^2}{2}\right)\right\}}_{\beta}. \tag{17}$$

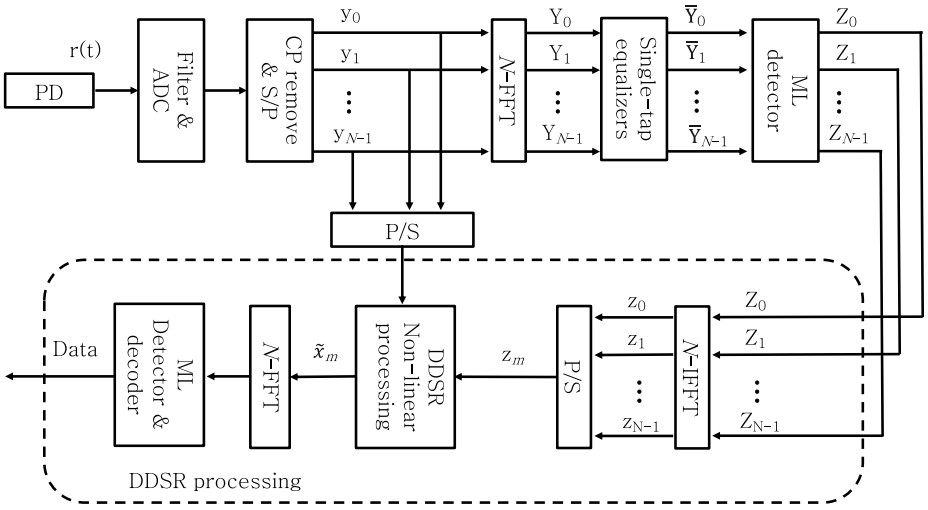

FIGURE 5. The block diagram of the DCO-OFDM receiver with DDSR processing.

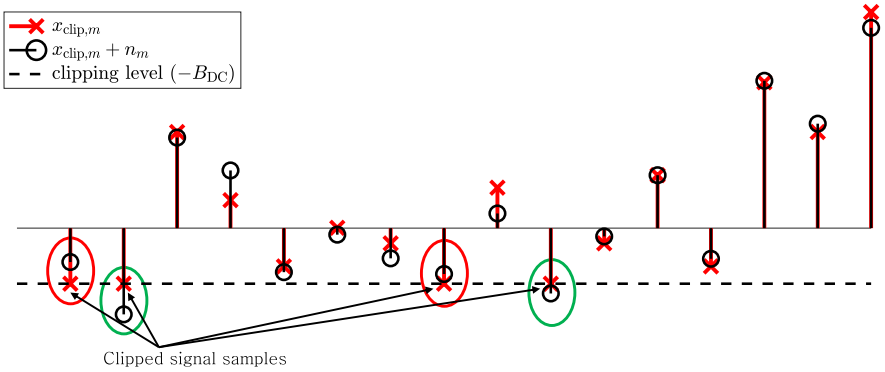

FIGURE 6. A time-domain signal sequence example.

case, the equalizer automatically corrects for constellation shrinkage. Note that the shrinkage may significantly affect signal detection especially in situations when the clipping level and/or the QAM modulation order are high. According to Bussgang's theorem, although the transmitted signal and the clipping noise are not correlated, this does not mean that they are independent. We have shown in [25] that useful information about the transmitted signal can be extracted from the clipping noise using a DDSR algorithm.

B. DDSR ALGORITHM

Next, we generalize the existing DDSR algorithms described in [21] and [25]. In the DDSR algorithm, preliminary decisions are made about the transmitted data and from these an estimate is made of the signal removed in the clipping operation. These estimated signals are then combined together with the original received signal to reconstruct/estimate the signal before clipping and thus to mitigate the clipping noise. This DDSR algorithm is shown in Fig. 5 and explained as follows:

1) The signal received by the photodetector, $y(t)$, is first filtered and passed through an analog to digital converter (ADC), and then sent into an FFT block to obtain the frequency domain signals, $\mathbf{Y} = [Y_0, Y_1, \ldots, Y_{N-1}]$.
2) The shrinking effect is eliminated by implementing an equalization step to Y_k by $\bar{Y}_k = \alpha^{-1} Y_k$.
3) The equalized frequency domain signal, $\bar{Y}_k$, is sent into an ML detector, and the output is

$$Z_k = \underset{X \in \mathbb{Z}_{M-\text{QAM}}}{\text{argmin}} \; ||\bar{Y}_k - X|| \tag{20}$$

where $\mathbb{Z}_{M-\text{QAM}}$ is the M-QAM constellation space, M is the QAM constellation size.
4) The detected frequency domain signal, Z_k, are converted into a time domain sequence, z_m, using IFFT. Note that the samples in $\mathbf{z} = [z_0, z_1, \ldots, z_{N-1}]$ would have both positive and negative peak values.
5) A new time domain sequence, $\tilde{x}_m$, is generated from y_m and z_m using DDSR algorithm by

$$\tilde{x}_m = \begin{cases} z_m, & \text{if } y_m \le \tau \\ y_m, & \text{if } y_m > \tau \end{cases} \tag{21}$$

where τ is the threshold used to direct the time-domain signal reconstruction. Using (21), the clipped signal samples in y_m are assumed to be replaced with z_m which would mitigate the effect of clipping distortion. In the DDSR algorithms described in [21] and [25], τ is fixed at the clipping level, $-B_{\mathrm{DC}}$. This would just provide the optimal performance when the transmitted signal is only subjected to the non-linear clipping distortion. However, when noise at receiver is also considered, the assumption that all the clipped signal samples in y_m will be replaced with z_m is not correct. For example, approximately half of the clipped samples in y_m would have values greater than $-B_{\mathrm{DC}}$ and would not be updated with z_m. This significantly limits the advantages of using the DDSR algorithm. Fig. 6 shows an example of a time-domain signal sequence to explain the influence of the noise on the signal reconstruction process. In this specific example, four signal samples are clipped at the transmitter. At the receiver, with the influence of the noise, two clipped signal samples are below the clipping level and another two clipped signal samples are above the clipping level. Using the existing DDSR algorithm, only signal samples below $-B_{\mathrm{DC}}$ (within the green circles) are updated with z_m. Two clipped signal samples which are above $-B_{\mathrm{DC}}$ (within the red circles) would not be successfully updated. In this paper, we generalize the description of the DDSR algorithm by not limiting its threshold at the clipping level. The optimal value of τ is studied in later sections using both theoretical analysis and Monte Carlo simulations.

6) Finally, $\tilde{x}_m$ is converted into frequency domain using FFT, and then sent into an ML detector to recover the transmitted data.

IV. DECISION ERROR NOISE IN DCO-OFDM

In the above described DDSR algorithm, the ML decision process in step 3 and IFFT process in step 4 are intended to restore most of the negative peaks of the signal which have been removed by clipping. Thus, replacing clipped signal samples will usually result in a more accurate estimate of the signal before clipping and the data recovered from this will have a lower BER. However, as explained in the previous section, the ML decisions in (20) are made with the detected signal subjected to both the noise generated at the receiver and the clipping distortion introduced at the transmitter and decision errors would normally occur. Therefore, the regenerated time-domain signal sequence in step 4, z_m, is not equal to the transmitted signal before clipping, x_m. We term the difference between x_m and z_m as decision error noise (DEN). The DEN is given by

$$e_m = x_m - z_m \tag{22}$$

In this section, we analyze the properties of the DEN noise which depend on a range of parameters including the signal power, the noise power, the clipping level, the QAM constellation size, M, and the number of OFDM subcarriers, N. We show that, when N is sufficiently large the DEN noise is approximately Gaussian. A theoretical analysis of its variance is presented which closely matches the simulation results. In the following, the SER performance of the conventional DCO-OFDM receiver is first determined and then used to calculate/estimate the number of OFDM subcarriers with detection errors. Based on these calculations, an expression for the variance of the DEN noise is obtained.

A. SER IN DCO-OFDM

We first calculate the error probability. The SER of any QAM based transmission systems can be tightly bounded using the pairwise error probability (PEP) [39] which can be also adapted to the case of DCO-OFDM. We use PEP($i \rightarrow j$) to denote the probability that the ith QAM constellation point is transmitted and the jth constellation point is received after performing ML decisions. Taking the shrinkage factor, the clipping noise and the AWGN noise into consideration, PEP($i \rightarrow j$) can be calculated using [39]

$$\mathrm{PEP}(i \rightarrow j) = Q\left(\frac{\alpha d_{ij}}{2\sigma_{\mathrm{o}}}\right) \tag{23}$$

where d_{ij} is the Euclidean distance between the ith QAM constellation point and the jth QAM constellation point, σ_{o} is the standard deviation of the sum of the clipping noise and AWGN. Since the clipping noise is independent of the AWGN, we can get

$$\sigma_{\mathrm{o}} = \sqrt{\sigma_{\mathrm{n}}^2 + \sigma_{\mathrm{c}}^2} \tag{24}$$

The SER, P_{s}, can be tightly upper bounded using [39]

$$\begin{aligned} P_{\mathrm{s}} &\leq \frac{1}{M}\sum_{i=1}^{M}\sum_{\substack{j=1 \\ j\neq i}}^{M}\mathrm{PEP}(i \rightarrow j) \\ &= \frac{1}{M}\sum_{i=1}^{M}\sum_{\substack{j=1 \\ j\neq i}}^{M} Q\left(\frac{\alpha d_{ij}}{2\sigma_{\mathrm{o}}}\right) \end{aligned} \tag{25}$$

In this paper, in line with most of the practical transmission scenarios, we considered a system in which the variance of the signal is much greater than the variance of the noise. Therefore, a reasonable assumption is made that the QAM constellation detection failure only occurs in the situation that the ML decision is made to the neighbors of the transmitted QAM constellation point. The neighbors of a constellation point means its adjacent points to which it has the shortest Euclidean distance and this is illustrated in in Fig. 7 for both 4-QAM and 16-QAM. In this case, P_{s} can be rewritten as

$$P_{\mathrm{s}} = K(M)Q\left(\frac{\alpha d}{2\sigma_{\mathrm{o}}}\right) \tag{26}$$

where

$$K(M) = 4\left(1 - \frac{1}{\sqrt{M}}\right) \tag{27}$$

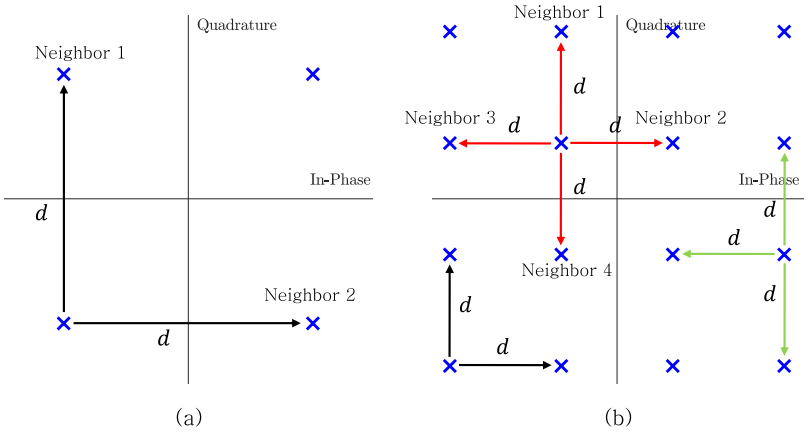

FIGURE 7. QAM constellation points and their 'neighbors', (a) 4-QAM, (b) 16-QAM.

is the average number of the neighbors of a QAM constellation point [39] when a square QAM constellation set is considered. d is the shortest Euclidean distance between two adjacent constellation points as shown in Fig. 7. d can be expressed as a function of the variance of the QAM constellation points, $E(|X_k|^2)$, using [39]

$$d = \sqrt{\frac{6E(|X_k|^2)}{M-1}} = \sqrt{\frac{6\sigma^2}{M-1}} \tag{28}$$

Finally, combining (17), (26), (27) and (28) gives

$$P_s = 4\left(1 - \frac{1}{\sqrt{M}}\right) Q\left(\sqrt{\frac{3\alpha^2}{2(M-1)\left(\beta + \frac{1}{\gamma}\right)}}\right) \tag{29}$$

where

$$\gamma = \frac{\sigma^2}{\sigma_n^2}, \tag{30}$$

and β is defined in (17). It can be seen from (29) that the SER is a function of the constellation size, the clipping ratio and the variance of the signal and the variance of AWGN.

We then present the SER results using both the theoretical analysis derived in (29) and Monte Carlo simulations. Different DC bias levels and thus different clipping levels are considered for both 4-QAM and 16-QAM. In Fig. 8, the SER is plotted as a function of γ with μ fixed at 0.5, 1, 2 and 3. It shows that the simulation result matches very well with the theoretical results obtained using (29). When the bias level is high, the SER decreases when γ increases. However, when the bias is low, clipping noise dominates and consequently the SER plot plateaus.

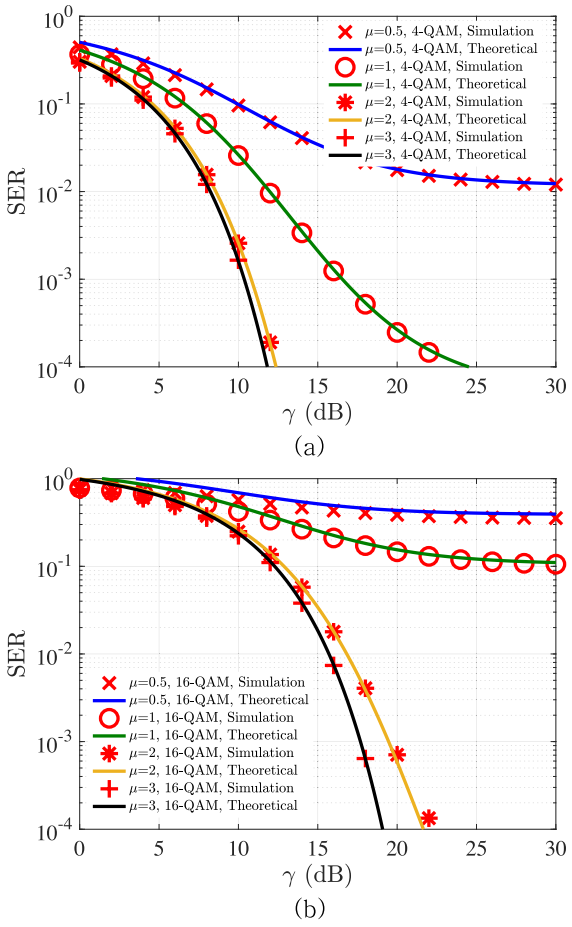

FIGURE 8. The theoretical and simulated SER plots, (a) 4-QAM, (b) 16-QAM.

B. THE VARIANCE OF DEN

Next, we analyze the variance of the DEN noise based the above detection error calculation. In an OFDM signal, when the overall number of subcarriers, N, is sufficiently large and the symbol error rate is P_s, the number of subcarriers with detection errors is less random and approximately NP_s. Consequently, the DEN noise, e_m, which is defined in (22) can be modelled as a multi-subcarrier signal with NP_s subcarriers which is added onto the transmitted signal before clipping. Moreover, since most of the incorrect decisions are made to the neighbours of the transmitted QAM constellation point,

each subcarrier of e_m is loaded with a 'point', χ, which has a Euclidean distance of d from its 'origin'. Therefore, z_m is given by

$$\begin{aligned} z_m &= \frac{1}{\sqrt{N}} \sum_{k=0}^{N-1} (X_k + \chi_k) \exp\left(\frac{j2\pi km}{N}\right) \\ &= \frac{1}{\sqrt{N}} \sum_{k=0}^{N-1} X_k \exp\left(\frac{j2\pi km}{N}\right) \\ &\quad + \frac{1}{\sqrt{N}} \sum_{k=0}^{N-1} \chi_k \exp\left(\frac{j2\pi km}{N}\right) \\ &= x_m + \frac{1}{\sqrt{N}} \sum_{k=0}^{N-1} \chi_k \exp\left(\frac{j2\pi km}{N}\right) \end{aligned} \tag{31}$$

and the time-domain DEN noise can be expressed as

$$e_m = -\frac{1}{\sqrt{N}} \sum_{k=0}^{N-1} \chi_k \exp\left(\frac{j2\pi km}{N}\right) \tag{32}$$

As discussed above, since χ_k has a distance of d from the origin of its Euclidean space, $E(|\chi_k|^2) = d^2$. Furthermore, because only NP_s subcarriers have errors, χ_k is zero on $N(1-P_s)$ OFDM subcarriers. Since the input and the output of the FFT/IFFT have the same average power as shown in Appendix-A, the following relationship can be obtained.

$$\begin{aligned} \sigma_e^2 &= \frac{E(|\chi_k|^2) \times NP_s + 0 \times N(1-P_s)}{N} \\ &= E(|\chi_k|^2) P_s \\ &= d^2 P_s \end{aligned} \tag{33}$$

Combining (28), (29), (33) gives

$$\sigma_e^2 = \frac{24\sigma^2}{M-1}\left(1 - \frac{1}{\sqrt{M}}\right) Q\left(\sqrt{\frac{3\alpha^2}{2(M-1)\left(\beta + \frac{1}{\gamma}\right)}}\right) \tag{34}$$

We then perform simulations to verify the theoretical analysis of the variance of the DEN noise. In the previous analysis, we predicted that the DEN noise will be Gaussian when the number of subcarriers which have detection errors is sufficiently large within one OFDM signal. Therefore, the statistical properties of the DEN noise are related to the power of the signal, the power of the noise, the signal clipping level and the number of the OFDM subcarrier. In Fig. 9, the PDF of the DEN noise is obtained using both simulations and the theoretical model derived in (34). In the simulations, γ is fixed at 20 dB and the μ is set to be 0.5. 4-QAM is used on each OFDM subcarrier. In Fig. 9 (a)-(d), different numbers of OFDM subcarriers are considered. We can see that the DEN noise becomes approximately Gaussian when the number of subcarriers is 512. Moreover, when the DEN noise is Gaussian, our theoretical analysis matches very well with the simulation results. In the following analysis, the number of OFDM subcarriers is fixed at 512. This large number of OFDM subcarriers can potentially lead to a high PAPR. However, we also study a system in which the clipping distortion or clipping noise is the main impairment and the transmitted signal is severely clipped. The benefit of this severe clipping operation is that it also limits the PAPR.

V. SNR PERFORMANCE

In this section, we analyze the SNR performance of the system when the DDSR algorithm is used for clipping noise mitigation. As shown in (21), the processed signal, $\tilde{x}_m$, is reconstructed using y_m and z_m and therefore encounters three types of noise. In particular, the signal samples reconstructed using y_m experience the AWGN noise and/or the clipping noise and the signal samples which are replaced with z_m are subject to the DEN noise. It can be noticed that the probability that a received signal sample is updated with y_m or z_m would affect the SNR of the processed signal and this probability depends on the choice of the DDSR threshold. In the following analysis, P_z is used to denote the probability that y_m is replaced with z_m in the signal reconstruction procedure and consequently $1 - P_z$ is the probability that y_m remains not being updated. P_z would depend on 1. the choice of the signal reconstruction threshold and 2. the statistical properties of the received signal. In order to obtain P_z, we first need to find the PDF of $x_{\text{clip},m} + n_m$, $p_{\text{cn}}(x)$. Since $x_{\text{clip},m}$ is independent of n_m, $p_{\text{cn}}(x)$ can be obtained using the convolution of $p_{\text{clip}}(x)$ shown in (14) and $p_{\text{n}}(x)$ shown in (19) and calculated using (35), as shown at the bottom of the page.

$$\begin{aligned} p_{\text{cn}}(x) &= \int_{-\infty}^{+\infty} p_{\text{n}}(x-\upsilon) p_{\text{clip}}(\upsilon) d\upsilon \\ &= \int_{-\infty}^{+\infty} \left(\frac{1}{\sqrt{2\pi}\sigma_{\text{n}}} \exp\left(-\frac{(x-\upsilon)^2}{2\sigma_{\text{n}}^2}\right) \left(\frac{1}{\sqrt{2\pi}\sigma} \exp\left(-\frac{\upsilon^2}{2\sigma^2}\right) h(\upsilon) + Q\left(\frac{B_{\text{DC}}}{\sigma}\right) \delta(\upsilon + B_{\text{DC}}) \right) \right) d\upsilon \\ &= Q\left(\frac{B_{\text{DC}}}{\sigma}\right) \frac{1}{\sqrt{2\pi}\sigma_{\text{n}}} \exp\left(-\frac{(B_{\text{DC}}+x)^2}{2\sigma_{\text{n}}}\right) + \int_{-B_{\text{DC}}}^{+\infty} \left(\frac{1}{2\pi\sigma\sigma_{\text{n}}} \exp\left(-\frac{(x-\upsilon)^2}{2\sigma_{\text{n}}^2}\right) \exp\left(-\frac{\upsilon^2}{2\sigma^2}\right) \right) d\upsilon \\ &= Q\left(\frac{B_{\text{DC}}}{\sigma}\right) \frac{1}{\sqrt{2\pi}\sigma_{\text{n}}} \exp\left(-\frac{(B_{\text{DC}}+x)^2}{2\sigma_{\text{n}}}\right) + \frac{1}{\sqrt{2\pi(\sigma^2+\sigma_{\text{n}}^2)}} \exp\left(-\frac{x^2}{2(\sigma+\sigma_{\text{n}}^2)}\right) Q\left(\frac{-(x+B_{\text{DC}})\sigma^2 - B_{\text{DC}}\sigma_{\text{n}}^2}{\sqrt{(\sigma^2+\sigma_{\text{n}}^2)\sigma^2\sigma_{\text{n}}^2}}\right) \end{aligned} \tag{35}$$

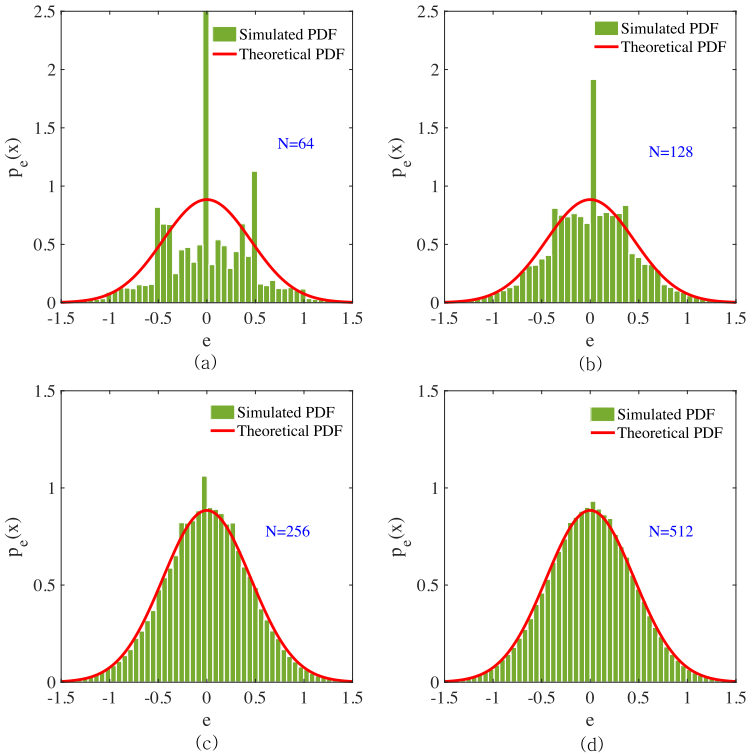

FIGURE 9. The PDF of the DEN noise obtained using both the theoretical model and simulations.

Then, the theoretical calculation shown in (35) is verified using simulations. Both the theoretical and the simulated PDFs of the clipped OFDM signal with AWGN noise are shown in Fig. 10. We can see from Fig. 10 that the statistical properties of the signal are affected by the variance of the AWGN noise. Also, the PDF changes when different values of B_{DC} or μ are considered. More importantly, it verifies that the PDFs obtained using the above theoretical analysis are very consistent with the simulated results. Note that, in DCO-OFDM, the bottom clipping ratio or B_{DC} is usually defined in dB as $10\log_{10}(\mu^2+1)$ dB [5], [17] which is also considered in this paper. Table-2 shows several examples of how μ is related to B_{DC} (in dB) with different values.

In the DDSR process, in order to replace most of the clipped signal samples in y_m with z_m, the DDSR threshold should be chosen at the clipping of $-B_{\mathrm{DC}}$ and with an offset. For example, in Fig. 6, all four clipped signal samples (rather than only two samples) can be successfully updated if the DDSR threshold is chosen to be slightly above $-B_{\mathrm{DC}}$. It can be noticed that the choice of this offset depends on the variance of the noise. To obtain more general conclusions, the offset coefficient is set relative to, σ_{n}, using $\eta\sigma_{\mathrm{n}}$. Then, the threshold becomes $-B_{\mathrm{DC}}+\eta\sigma_{\mathrm{n}}$ and signal reconstruction operation shown in (21) is rewritten as

$$\tilde{x}_m = \begin{cases} z_m, & \text{if } y_m \le -B_{\mathrm{DC}} + \eta\sigma_{\mathrm{n}} \\ y_m, & \text{if } y_m > -B_{\mathrm{DC}} + \eta\sigma_{\mathrm{n}} \end{cases} \tag{36}$$

Note that, in a practical transmission system, in order to implement (36), the variance of the AWGN is required to be pre-estimated at the receiver side and the optimal value of η is obtained in the following analysis.

Next, the probability that the received signal samples (including both the clipped signal samples and the unclipped signal samples) are below the signal reconstruction threshold, P_{z}, can be obtained using (37), as shown at the bottom of the page. In (37), $P_{\mathrm{z},1}$ is the probability that a transmitted signal sample is clipped and this clipped signal sample has a value below the DDSR threshold after the influence of the AWGN noise. This is because $Q\left(B_{\mathrm{DC}}/\sigma\right)$ is the probability that a transmitted signal sample is clipped and $1-Q\left(\eta\sigma_{\mathrm{n}}/\sigma_{\mathrm{n}}\right)$

$$\begin{aligned} P_{\mathrm{z}} &= \int_{-\infty}^{-B_{\mathrm{DC}}+\eta\sigma_{\mathrm{n}}} p_{\mathrm{cn}}(x)dx \\ &= \underbrace{(1-Q(\eta))Q\left(\frac{B_{\mathrm{DC}}}{\sigma}\right)}_{P_{\mathrm{z},1}} + \underbrace{\frac{1}{\sqrt{2\pi(\sigma^2+\sigma_{\mathrm{n}}^2)}}\int_{-\infty}^{-B_{\mathrm{DC}}+\eta\sigma_{\mathrm{n}}} \exp\left(-\frac{x^2}{2(\sigma^2+\sigma_{\mathrm{n}}^2)}\right) Q\left(\frac{-(x+B_{\mathrm{DC}})\sigma^2 - B_{\mathrm{DC}}\sigma_{\mathrm{n}}^2}{\sqrt{(\sigma^2+\sigma_{\mathrm{n}}^2)\sigma^2\sigma_{\mathrm{n}}^2}}\right)dx}_{P_{\mathrm{z},2}} \end{aligned} \tag{37}$$

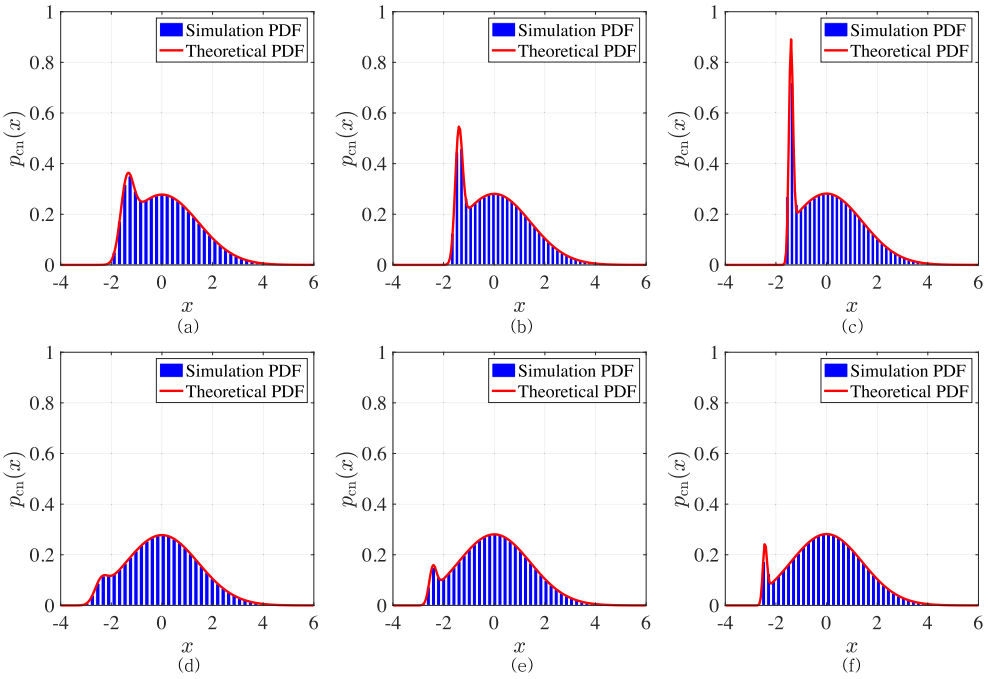

FIGURE 10. The PDF fo the clipped signal with the influence of Gaussian noise, (a). $B_{DC} = 3$ dB, $\gamma = 15$ dB, (b). $B_{DC} = 3$ dB, $\gamma = 20$ dB, (c). $B_{DC} = 3$ dB, $\gamma = 25$ dB, (d). $B_{DC} = 6$ dB, $\gamma = 15$ dB, (e). $B_{DC} = 6$ dB, $\gamma = 20$ dB, (f). $B_{DC} = 6$ dB, $\gamma = 25$ dB.

is the probability that the value of a clipped sample is below the DDSR threshold after AWGN noise is added. $P_{z,2}$ is the probability that a transmitted signal sample is unclipped and this unclipped signal sample has a value below the DDSR threshold after the influence of the AWGN noise. Since only the signal samples which are updated using z_m are affected by the DEN noise and the updating probability is P_z, the variance of the DEN noise in $\tilde{x}_m$ is $\sigma_e^2 P_z$. Similarly, $1 - P_z$ is the ratio/probability of the signal samples which are not updated and therefore remain being affected by AWGN. Consequently, the variance of the AWGN in $\tilde{x}_m$ is $\sigma_n^2(1 - P_z)$. Furthermore, after implementing the signal reconstruction procedure shown in (36), the shrinkage ratio increases since the number of clipped signal samples are reduced. The probability that a clipped signal sample is above the DDSR threshold and therefore remaining being clipped is $Q(\eta\sigma_n/\sigma_n)$. Taking this into account, the new shrinkage factor, α_{new}, becomes

$$\alpha_{new} = 1 - Q\left(\frac{\eta\sigma_n}{\sigma_n}\right) Q\left(\frac{B_{DC}}{\sigma}\right) = 1 - Q(\eta) + \alpha Q(\eta) \tag{38}$$

and the variance of the clipping noise becomes $Q(\eta)\sigma_c^2$. Taking all these factors into account, the SNR of the processed signal can be given by

$$\gamma_o(\eta) = \frac{\alpha_{new}^2 \sigma^2}{\sigma_e^2 P_z + \sigma_n^2(1 - P_z) + Q(\eta)\sigma_c^2} \tag{39}$$

which is shown to be a function of η and therefore the DDSR threshold. Note that when the DDSR threshold is extremely high, the reconstructed signal, $\tilde{x}_m$, would be exactly z_m. Also, when the DDSR threshold is extremely low, $\tilde{x}_m$ would be y_m. Both z_m and y_m would be decoded with the same performance. Therefore, we predict that there is a value of η which can provide the optimal performance.

TABLE 2. Several examples of μ and B_{DC} (in dB).

μ	0.5	0.76	1	1.73	2	3
B_{DC} (in dB)	1	2	3	6	7	10

In Fig. 11, the theoretical SNR is plotted as a function of η with γ fixed at different values. In these results, in order to see the effectiveness of the studied algorithm on mitigating clipping noise, clipping noise rather than the AWGN noise is the dominant noise source. Consequently, the added DC biases are low so that the transmitted data cannot be successfully decoded using conventional receiver processing. In these plots, the DC bias is set by 1 dB for 4-QAM and 4 dB for 16-QAM. It can be seen from Fig. 11 that the SNR of the processed signal significantly depends on η. The SNR first increases and then decreases when η is increased from 0 to 10. Note that $\eta = 0$ is related to the previous DDSR method in which the signal reconstruction threshold is fixed at $-B_{DC}$. The value of η which can maximize the SNR varies as γ changes. When γ is changed from 21 dB to 30 dB, the optimal η varies from 2 to 3.5.

This approach of using the theoretical SNR to locate the optimum DDSR thresholds can be implemented efficiently

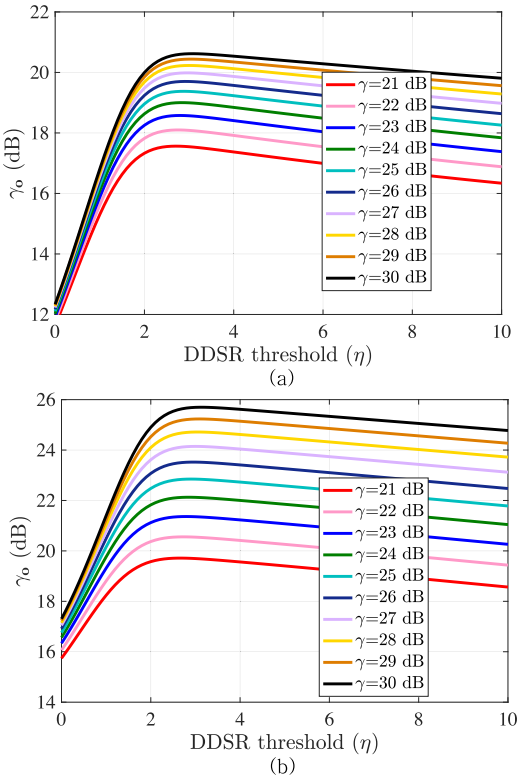

FIGURE 11. The SNR obtained based on theoretical analysis for different DDSR thresholds (a). 4-QAM $B_{DC} = 1$ dB, (b). 16-QAM $B_{DC} = 4$ dB.

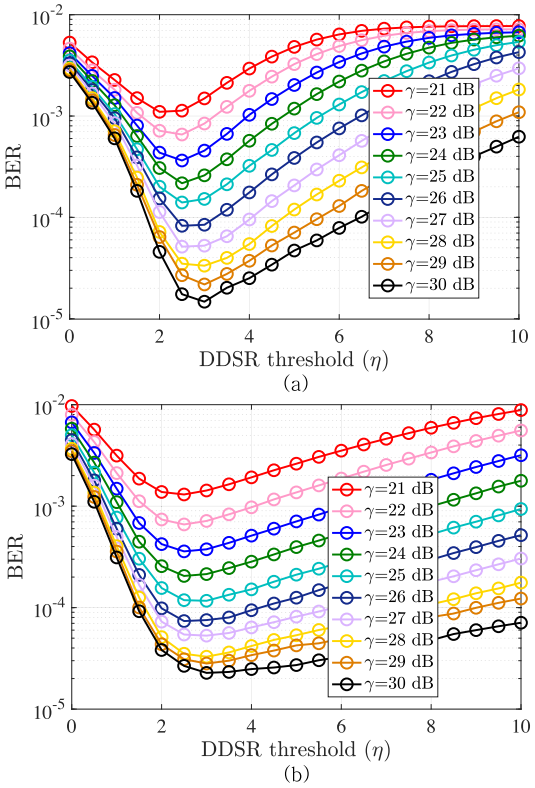

FIGURE 12. The BER obtained based on Monte Carlo simulations for different DDSR thresholds (a). 4-QAM $B_{DC} = 1$ dB, (b). 16-QAM $B_{DC} = 4$ dB.

without a significant amount of simulations. However, the SNR in (39) is defined in the time domain while the ML decisions are made in the frequency domain. Unlike AWGN noise, both the clipping noise and the DEN noise after the time domain signal reconstruction no longer have a Gaussian-like form when the signal is transformed back to the frequency domain (see Fig. 3 (c) in [25]). Therefore, the variances of the clipping noise and the DEN noise cannot precisely indicate the their actual influence on the signal detection process. Also, because of this reason, the classical formulas used to show the relationship between BER and SNR in an AWGN channel do not apply in this situation.

VI. MONTE CARLO SIMULATION RESULTS

In this section, Monte Carlo simulations are performed to locate the optimal DDSR thresholds which can provide the minimum BER. In Fig. 12, the BER is simulated as a function of η with γ fixed at different values. It can be seen that the BER first decreases and then increases when η increases. The optimal DDSR threshold which can minimize the BER varies slightly for different values of γ. More importantly, comparing Fig. 12 to Fig. 11, we can notice that the optimal DDSR thresholds obtained using Monte Carlo simulations have almost identical values with those found using theoretical SNR analysis especially when γ becomes large.

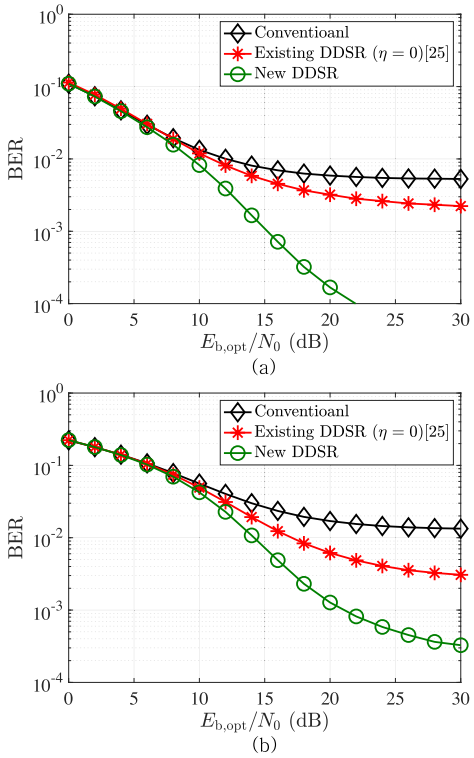

FIGURE 13. The simulated BER plotted as a function of $E_{b,opt}/N_0$ (a). 4-QAM $B_{DC} = 1$ dB, (b). 16-QAM $B_{DC} = 4$ dB.

Next, we show the BER performance of overall transmission when the DDSR algorithm is used with optimal thresholds. Its performance is compared to both the conventional receiver and the previous clipping noise mitigation receiver in which the signal reconstruction thresholds are fixed at the clipping levels. In these simulations, the transmitted optical power is set to unity and the BER is simulated as a function of $E_{\mathrm{b,opt}}/N_0$. $E_{\mathrm{b,opt}}$ is the transmitted optical energy per bit and given by

$$E_{\mathrm{b,opt}} = \frac{P_{\mathrm{opt}}}{b} \tag{40}$$

where b is the transmission bit rate and N_0 is the single-sided noise power spectral density. In these simulations, both 4-QAM and 16-QAM are considered. As shown in Fig. 13, compared to the conventional receiver, although the receiver using previous DDSR clipping noise mitigation can improve the performance of the system, the BER has a plateau level at which the BER would not decrease as $E_{\mathrm{b,opt}}/N_0$ increases. Using the receiver with optimal clipping noise mitigation can significantly improve the performance of the system for both 4-QAM and 16-QAM and also avoid the BER plateau level for 4-QAM.

VII. CONCLUSION

In this paper, we study the performance of an enhanced time-domain based DDSR algorithm which has a flexible signal reconstruction threshold for the mitigation of clipping noise in optical OFDM systems. We show that, although using the previous DDSR algorithm can mitigate the clipping noise in DCO-OFDM, the performance of the system remains being severely affected when the added DC bias is too low. Due to the impacts of the unavoidable noise at the receiver, fixing the signal reconstruction threshold at the clipping level is not an optimal solution and can limit the advantages of this DDSR algorithm. In this paper, we study how the ML detections performed in the frequency-domain affects the regenerated time-domain signal sequence by introducing the DEN noise. Furthermore, by analyzing how the variances of the clipping noise, the AWGN and the DEN noise are affected after the time-domain signal reconstruction, a theoretical SNR expression of the processed signal is calculated which can be used to efficiently locate the optimal DDSR threshold. Finally, Monte Carlo simulations are performed to show the advantages of using this method compared to both the conventional receiver and the previous DDSR algorithm.

APPENDIX A
THE CALCULATION OF $E(|X|^2) = \sigma^2$

The IFFT in (1) is paired with the FFT given by

$$X_k = \frac{1}{\sqrt{N}} \sum_{m=0}^{N-1} x_m \exp\Big(-\frac{j2\pi mk}{N}\Big), \quad \text{for } 0 \le k \le N-1 \tag{41}$$

Based on (41), $E(|X_k|^2)$ can be calculated as

$$\begin{aligned} E(|X_k|^2) &= E(X_k X_k^*) \\ &= E\left(\frac{1}{\sqrt{N}} \sum_{m=0}^{N-1} x_m \exp\Big(-\frac{j2\pi mk}{N}\Big) \right. \\ &\quad \left. \times \left(\frac{1}{\sqrt{N}} \sum_{p=0}^{N-1} x_p \exp\Big(-\frac{j2\pi pk}{N}\Big)\right)^*\right) \\ &= E\left(\frac{1}{N} \sum_{m=0}^{N-1}\sum_{p=0}^{N-1} x_m x_p^* \exp\Big(-\frac{j2\pi (m-p)k}{N}\Big)\right) \\ &= \frac{1}{N} \sum_{m=0}^{N-1}\sum_{p=0}^{N-1} E(x_m x_p^*) \exp\Big(-\frac{j2\pi (m-p)k}{N}\Big) \end{aligned} \tag{42}$$

Since $E(x_m x_p^*) = 0$ when $m \neq p$, $E(|X_k|^2)$ is then further calculated as

$$E(|X_k|^2) = \frac{1}{N} \sum_{m=0}^{N-1} E(|x_m|^2) = E(x_m^2) = \sigma^2 \tag{43}$$

Consequently, using the specific form of the IFFT/FFT pair shown in (1) and (41), the discrete signals at the input and the output of the transform have the same average power.

APPENDIX B
THE CALCULATIONS OF THE VARIANCE OF THE CLIPPING NOISE AND THE OPTICAL POWER FOR DOUBLE-SIDED CLIPPED OPTICAL OFDM SIGNALS

In order to obtain the variance of the clipping noise, σ_{c}^2, we first need to calculate the variance of x_{clip}, $\sigma_{x_{\mathrm{clip}}}^2$. Then, based on the relationship shown in (10), σ_{c}^2 can be determined using

$$\sigma_{\mathrm{c}}^2 = \sigma_{x_{\mathrm{clip}}}^2 - \alpha^2\sigma^2. \tag{44}$$

Because the mean of $x_{\mathrm{clip},m}$ is not zero due to the non-linear clipping operation, both the mean of $x_{\mathrm{clip},m}$, $m_{x_{\mathrm{clip}}}$ and $E(x_{\mathrm{clip}}^2)$ need to be calculated first to get $\sigma_{x_{\mathrm{clip}}}^2$. $E(x_{\mathrm{clip}}^2)$ is calculated as

$$\begin{aligned} E(x_{\mathrm{clip}}^2) &= \int_{-\infty}^{+\infty} x^2 p_{x_{\mathrm{clip}}}(x)dx \\ &= B_{\mathrm{DC}}^2 Q\left(\frac{B_{\mathrm{DC}}}{\sigma}\right) + \lambda^2 Q\Big(\frac{\lambda}{\sigma}\Big) + \int_{-B_{\mathrm{DC}}}^{\lambda} x^2 p_{x_{\mathrm{clip}}}(x)dx \\ &= \sigma^2\mu^2 Q(\mu) + \sigma^2\rho^2 Q(\rho) + \underbrace{\int_{-B_{\mathrm{DC}}}^{\lambda} x^2 p_{x_{\mathrm{clip}}}(x)dx}_{\zeta} \end{aligned} \tag{45}$$

where ζ is calculated in (46), as shown at the top of the next page. Combining (45) and (46) gives

$$\begin{aligned} E(x_{\mathrm{clip}}^2) = \sigma^2\Big[&\mu^2 Q(\mu) + \rho^2 Q(\rho) \\ &- \frac{1}{\sqrt{2\pi}}\left(\rho \exp\left(-\frac{\rho^2}{2}\right) + \mu \exp\left(-\frac{\mu^2}{2}\right)\right) + \alpha\Big] \end{aligned} \tag{47}$$

$$\begin{aligned}\zeta &= \frac{1}{\sqrt{2\pi}\sigma}\int_{-B_{\mathrm{DC}}}^{\lambda} x^2 \exp\Big(-\frac{x^2}{2\sigma^2}\Big)dx \\ &= -\frac{\sigma}{\sqrt{2\pi}}\int_{-B_{\mathrm{DC}}}^{\lambda} x d\exp\Big(-\frac{x^2}{2\sigma^2}\Big) \\ &= -\frac{\sigma}{\sqrt{2\pi}}\lambda\exp\Big(-\frac{\lambda^2}{2\sigma^2}\Big) - \frac{\sigma}{\sqrt{2\pi}}B_{\mathrm{DC}}\exp\Big(-\frac{B_{\mathrm{DC}}^2}{2\sigma^2}\Big) + \frac{\sigma^2}{\sqrt{2\pi}\sigma}\int_{-B_{\mathrm{DC}}}^{\lambda}\exp\Big(-\frac{x^2}{2\sigma^2}\Big)dx \\ &= -\frac{\sigma}{\sqrt{2\pi}}\lambda\exp\Big(-\frac{\lambda^2}{2\sigma^2}\Big) - \frac{\sigma}{\sqrt{2\pi}}B_{\mathrm{DC}}\exp\Big(-\frac{B_{\mathrm{DC}}^2}{2\sigma^2}\Big) + \sigma^2\Big[1 - Q\Big(\frac{B_{\mathrm{DC}}}{\sigma}\Big) - Q\Big(\frac{\lambda}{\sigma}\Big)\Big] \\ &= \sigma^2\Big(-\frac{\rho}{\sqrt{2\pi}}\exp\Big(-\frac{\rho^2}{2}\Big) - \frac{\mu}{\sqrt{2\pi}}\exp\Big(-\frac{\mu^2}{2}\Big) + \alpha\Big)\end{aligned} \tag{46}$$

$$\begin{aligned}\sigma_{x_{\mathrm{clip}}}^2 &= E(x_{\mathrm{clip}}^2) - m_{x_{\mathrm{clip}}}^2 \\ &= \sigma^2\Big\{\mu^2 Q(\mu) + \rho^2 Q(\rho) - \frac{1}{\sqrt{2\pi}}\Big(\rho\exp\Big(-\frac{\rho^2}{2}\Big) + \mu\exp\Big(-\frac{\mu^2}{2}\Big)\Big) + \alpha \\ &\quad - \Big[\rho Q(\rho) - \mu Q(\mu) - \frac{1}{\sqrt{2\pi}}\Big(\exp\Big(-\frac{\rho^2}{2}\Big) - \exp\Big(-\frac{\mu^2}{2}\Big)\Big)\Big]^2\Big\}\end{aligned} \tag{49}$$

Next, the mean of x_{clip} is calculated as

$$\begin{aligned}m_{x_{\mathrm{clip}}} &= E(x_{\mathrm{clip}}) \\ &= \int_{-\infty}^{+\infty} x p_{x_{\mathrm{clip}}}(x)dx \\ &= -B_{\mathrm{DC}}Q\Big(\frac{B_{\mathrm{DC}}}{\sigma}\Big) - \frac{\sigma}{\sqrt{2\pi}}\exp\Big(-\frac{\lambda^2}{2\sigma^2}\Big) \\ &\quad + \frac{\sigma}{\sqrt{2\pi}}\exp\Big(-\frac{B_{\mathrm{DC}^2}}{2\sigma^2}\Big) + \lambda Q\Big(\frac{\lambda}{\sigma}\Big) \\ &= -\sigma\mu Q(\mu) - \frac{\sigma}{\sqrt{2\pi}}\exp\Big(-\frac{\rho^2}{2}\Big) \\ &\quad + \frac{\sigma}{\sqrt{2\pi}}\exp\Big(-\frac{\mu^2}{2}\Big) + \sigma\rho Q(\rho) \\ &= \sigma\Big[\rho Q(\rho) - \mu Q(\mu) \\ &\quad - \frac{1}{\sqrt{2\pi}}\Big(\exp\Big(-\frac{\rho^2}{2}\Big) - \exp\Big(-\frac{\mu^2}{2}\Big)\Big)\Big]\end{aligned} \tag{48}$$

Then, the variance of $x_{\mathrm{clip},m}$ is calculated using (49), as shown at the top of the page. Furthermore, based on (44), the variance of the clipping noise is obtained using

$$\begin{aligned}\sigma_{\mathrm{c}}^2 &= \sigma_{x_{\mathrm{clip}}}^2 - \alpha^2\sigma^2 \\ &= \sigma^2\Big\{\mu^2 Q(\mu) + \rho^2 Q(\rho) \\ &\quad - \frac{1}{\sqrt{2\pi}}\Big(\rho\exp(-\frac{\rho^2}{2}) + \mu\exp(-\frac{\mu^2}{2})\Big) \\ &\quad - \Big[\rho Q(\rho) - \mu Q(\mu) - \frac{1}{\sqrt{2\pi}}\Big(\exp(-\frac{\rho^2}{2}) - \exp(-\frac{\mu^2}{2})\Big)\Big]^2 \\ &\quad + \alpha(1-\alpha)\Big\}\end{aligned} \tag{50}$$

The transmitted optical power is the mean of $s_{\mathrm{DCO},m}$ which can be obtained using

$$\begin{aligned}P_{\mathrm{opt}} &= \int_{-\infty}^{+\infty} x p_{x_{\mathrm{clip}}}(x)dx + B_{\mathrm{DC}} \\ &= m_{x_{\mathrm{clip}}} + B_{\mathrm{DC}} \\ &= \sigma\Big[\rho Q(\rho) - \mu Q(\mu) \\ &\quad - \frac{1}{\sqrt{2\pi}}\Big(\exp(-\frac{\rho^2}{2}) - \exp(-\frac{\mu^2}{2})\Big)\Big] + \sigma\mu \\ &= \sigma\Big\{\rho Q(\rho) - \mu[Q(\mu) - 1] \\ &\quad - \frac{1}{\sqrt{2\pi}}\Big(\exp(-\frac{\rho^2}{2}) - \exp(-\frac{\mu^2}{2})\Big)\Big\}\end{aligned} \tag{51}$$

ACKNOWLEDGMENT

Part of this work was performed when Dr. Cuiwei He was with Monash University and supported by an Australian Research Council (ARC) Discovery funding scheme (DP150100003). The authors also want to thank Prof. Jean Armstrong for her valuable suggestions at the initial stage of this work.

REFERENCES

[1] J. Armstrong, "OFDM for optical communications," *J. Lightw. Technol.*, vol. 27, no. 3, pp. 189–204, Feb. 1, 2009.
[2] D. O'Brien, S. Rajbhandari, and H. Chun, "Transmitter and receiver technologies for optical wireless," *Phil. Trans. Roy. Soc. A, Math., Phys. Eng. Sci.*, vol. 378, no. 2169, Apr. 2020, Art. no. 20190182.
[3] H. Haas, L. Yin, Y. Wang, and C. Chen, "What is LiFi?" *J. Lightw. Technol.*, vol. 34, no. 6, pp. 1533–1544, Mar. 15, 2016.
[4] J. Armstrong and A. J. Lowery, "Power efficient optical OFDM," *Electron. Lett.*, vol. 42, no. 6, pp. 370–372, Mar. 2006.
[5] S. D. Dissanayake and J. Armstrong, "Comparison of ACO-OFDM, DCO-OFDM and ADO-OFDM in IM/DD systems," *J. Lightw. Technol.*, vol. 31, no. 7, pp. 1063–1072, Apr. 1, 2013.

[6] B. Ranjha and M. Kavehrad, "Hybrid asymmetrically clipped OFDM-based IM/DD optical wireless system," *IEEE/OSA J. Opt. Commun. Netw.*, vol. 6, no. 4, pp. 387–396, Apr. 2014.
[7] S. C. J. Lee, S. Randel, F. Breyer, and A. M. J. Koonen, "PAM-DMT for intensity-modulated and direct-detection optical communication systems," *IEEE Photon. Technol. Lett.*, vol. 21, no. 23, pp. 1749–1751, Dec. 1, 2009.
[8] R. Mesleh, H. Elgala, and H. Haas, "On the performance of different OFDM based optical wireless communication systems," *IEEE/OSA J. Opt. Commun. Netw.*, vol. 3, no. 8, pp. 620–628, Aug. 2011.
[9] N. Fernando, Y. Hong, and E. Viterbo, "Flip-OFDM for unipolar communication systems," *IEEE Trans. Commun.*, vol. 60, no. 12, pp. 3726–3733, Dec. 2012.
[10] H. Elgala and T. D. C. Little, "P-OFDM: Spectrally efficient unipolar OFDM," in *Proc. Opt. Fiber Commun. Conf.*, 2014, pp. 1–3.
[11] D. Tsonev, S. Sinanovic, and H. Haas, "Novel unipolar orthogonal frequency division multiplexing (U-OFDM) for optical wireless," in *Proc. IEEE 75th Veh. Technol. Conf. (VTC Spring)*, May 2012, pp. 1–5.
[12] Q. Wang, C. Qian, X. Guo, Z. Wang, D. G. Cunningham, and I. H. White, "Layered ACO-OFDM for intensity-modulated direct-detection optical wireless transmission," *Opt. Exp.*, vol. 23, no. 9, pp. 12382–12393, May 2015.
[13] L. Chen, B. Krongold, and J. Evans, "Successive decoding of anti-periodic OFDM signals in IM/DD optical channel," in *Proc. IEEE Int. Conf. Commun.*, May 2010, pp. 1–6.
[14] D. Tsonev, S. Videv, and H. Haas, "Unlocking spectral efficiency in intensity modulation and direct detection systems," *IEEE J. Sel. Areas Commun.*, vol. 33, no. 9, pp. 1758–1770, Sep. 2015.
[15] A. J. Lowery, "Comparisons of spectrally-enhanced asymmetrically-clipped optical OFDM systems," *Opt. Exp.*, vol. 24, no. 4, pp. 3950–3966, Feb. 2016.
[16] L. Chen, B. Krongold, and J. Evans, "Diversity combining for asymmetrically clipped optical OFDM in IM/DD channels," in *Proc. IEEE Global Telecommun. Conf. (GLOBECOM)*, Nov. 2009, pp. 1–6.
[17] L. Chen, B. Krongold, and J. Evans, "Theoretical characterization of nonlinear clipping effects in IM/DD optical OFDM systems," *IEEE Trans. Commun.*, vol. 60, no. 8, pp. 2304–2312, Aug. 2012.
[18] S. Dimitrov, S. Sinanovic, and H. Haas, "Clipping noise in OFDM-based optical wireless communication systems," *IEEE Trans. Commun.*, vol. 60, no. 4, pp. 1072–1081, Apr. 2012.
[19] Z. Zhang, A. Chaaban, and M.-S. Alouini, "Residual clipping noise in multi-layer optical OFDM: Modeling, analysis, and applications," *IEEE Trans. Wireless Commun.*, vol. 19, no. 9, pp. 5846–5859, Sep. 2020.
[20] B. Song, B. Corcoran, Q. Wang, L. Zhuang, and A. J. Lowery, "Subcarrier pairwise coding for short-haul L/E-ACO-OFDM," *IEEE Photon. Technol. Lett.*, vol. 29, no. 18, pp. 1584–1587, Sep. 15, 2017.
[21] D. Kim and G. L. Stübler, "Clipping noise mitigation for OFDM by decision-aided reconstruction," *IEEE Commun. Lett.*, vol. 3, no. 1, pp. 4–6, Jan. 1999.
[22] J. Tellado, L. M. C. Hoo, and J. M. Cioffi, "Maximum-likelihood detection of nonlinearly distorted multicarrier symbols by iterative decoding," *IEEE Trans. Commun.*, vol. 51, no. 2, pp. 218–228, Feb. 2003.
[23] A. W. Azim, Y. L. Guennec, and G. Maury, "Enhanced DC-biased optical OFDM for intensity-modulated optical OFDM access systems," in *Proc. 18th Int. Conf. Transparent Opt. Netw. (ICTON)*, Jul. 2016, pp. 1–4.
[24] A. W. Azim, Y. L. Guennec, and G. Maury, "OFDM for optical wireless systems under severe clipping conditions," in *Proc. Adv. Wireless Opt. Commun. (RTUWO)*, Nov. 2016, pp. 201–206.
[25] C. He and J. Armstrong, "Clipping noise mitigation in optical OFDM systems," *IEEE Commun. Lett.*, vol. 21, no. 3, pp. 548–551, Mar. 2016.
[26] A. W. Azim, Y. L. Guennec, and G. Maury, "Decision-directed iterative methods for PAPR reduction in optical wireless OFDM systems," *Opt. Commun.*, vol. 389, pp. 318–330, Apr. 2017.
[27] T. Q. Wang, H. Li, and X. Huang, "Analysis and mitigation of clipping noise in layered ACO-OFDM based visible light communication systems," *IEEE Trans. Commun.*, vol. 67, no. 1, pp. 564–577, Jan. 2018.
[28] C. Li, Z. Xu, C. Yang, Q. Yang, and S. Yu, "Experimental demonstration of clipping noise mitigation for OFDM-based underwater optical wireless communications," in *Proc. Asia Commun. Photon. Conf.*, 2017, pp. 1–3.
[29] M. Zhang and Z. Zhang, "An optimum DC-biasing for DCO-OFDM system," *IEEE Commun. Lett.*, vol. 18, no. 8, pp. 1351–1354, Aug. 2014.
[30] C. Chen, S. Videv, D. Tsonev, and H. Haas, "Fractional frequency reuse in DCO-OFDM-based optical attocell networks," *J. Lightw. Technol.*, vol. 33, no. 19, pp. 3986–4000, Oct. 1, 2015.
[31] C. He, Z. Ahmed, and S. Collins, "Optical OFDM and SiPM receivers," in *Proc. IEEE Globecom Workshops (GC Wkshps)*, Dec. 2020, pp. 1–6.
[32] C. He, Z. Ahmed, and S. Collins, "Signal pre-equalization in a silicon photomultiplier-based optical OFDM system," *IEEE Access*, vol. 9, pp. 23344–23356, 2021.
[33] Y. Li, M. Safari, R. Henderson, and H. Haas, "Nonlinear distortion in SPAD-based optical OFDM systems," in *Proc. IEEE Globecom Workshops (GC Wkshps)*, Dec. 2015, pp. 1–6.
[34] Y. Li, M. Safari, R. Henderson, and H. Haas, "Optical OFDM with single-photon avalanche diode," *IEEE Photon. Technol. Lett.*, vol. 27, no. 9, pp. 943–946, May 1, 2015.
[35] J. Armstrong, "Peak-to-average power reduction for OFDM by repeated clipping and frequency domain filtering," *Electron. Lett.*, vol. 38, no. 5, pp. 246–247, 2002.
[36] J. J. Bussgang, "Crosscorrelation functions of amplitude-distorted Gaussian signals," Res. Lab. Electron., Massachusetts Inst. Technol., Cambridge, MA, USA, Tech. Rep. 216, 1952.
[37] J. M. Kahn and J. R. Barry, "Wireless infrared communications," *Proc. IEEE*, vol. 85, no. 2, pp. 265–298, Feb. 1997.
[38] B. C. Jeffrey and M. K. Joseph, "Modeling of nondirected wireless infrared channels," *IEEE Trans. Commun.*, vol. 45, no. 10, pp. 1260–1268, Oct. 1997.
[39] J. G. Proakis and M. Salehi, *Digital Communications*. New York, NY, USA: McGraw-Hill, 1995.

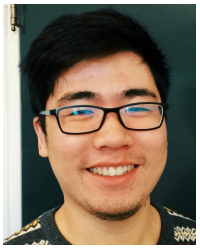

CUIWEI HE received the Ph.D. degree in optical wireless communication from Monash University, Melbourne, Australia, in 2017. From 2017 to 2020, he worked as a Research Fellow with Monash University. From 2020 to 2021, he was a Postdoctoral Research Assistant with the Department of Engineering Science, University of Oxford, U.K. He is currently an Assistant Professor with the School of Information Science, Japan Advanced Institute of Science and Technology (JAIST). His research interests include visible light communication, visible light positioning, optical wireless communication, multiple-input multiple-output (MIMO) technology, optical orthogonal frequency division multiplexing (OFDM), and optical receiver design.

YUTO LIM (Member, IEEE) received the B.Eng. (Hons.) and M.Inf.Tech. degrees from Universiti Malaysia Sarawak (UNIMAS), Malaysia, in 1998 and 2000, respectively, and the Ph.D. degree in communications and computer engineering from Kyoto University, in 2005. In November 2005, he was an Expert Researcher with the National Institute of Information and Communications Technology (NICT), Japan, until September of 2009. In 2005, he was actively joining the standardization activities of IEEE 802.11s Mesh Networking. He and his team members have introduced two proposals which are currently adopted in the draft of IEEE 802.11s D1.04. He also led the RA-OLSR group in resolving a part of the comments. In 2006, he was also actively joining the standardization activities of next-generation home networks from Telecommunication Technology Committee (TTC), Japan. Since October 2009, he has been working with Japan Advanced Institute of Science and Technology (JAIST), as an Associate Professor. From 2017 to 2019, he was actively joining the standardization activities of smart cities from the Bridging the Standardization Gap (BSG) Working Group of the TTC, Japan. He is honorably appointed as a TTC Representative to report the "Smart City" activities in Asia Pacific Region in both APT Standardization Program Forum (ASTAP) and APT Telecommunication/ICT Development Forum (ADF). His research interests include smart homes, smart cities, cyber-physical systems, the Internet of Things, future wireless communication and networks, wireless network coding, and smart energy distribution. He is a member of IEICE and IPSJ.